

Improved torque formula for low and intermediate mass planetary migration

María Alejandra Jiménez [★] and Frédéric S. Masset

Instituto de Ciencias Físicas, Universidad Nacional Autónoma de México, Av. Universidad s/n, 62210 Cuernavaca, Mor., Mexico

Accepted 2017 July 27. Received 2017 July 27; in original form 2017 April 25

ABSTRACT

The migration of planets on nearly circular, non-inclined orbits in protoplanetary discs is entirely described by the disc’s torque. This torque is a complex function of the disc parameters, and essentially amounts to the sum of two components: the Lindblad torque and the corotation torque. Known torque formulae do not reproduce accurately the torque actually experienced in numerical simulations by low- and intermediate-mass planets in radiative discs. One of the main reasons for this inaccuracy is that these formulae have been worked out in two-dimensional analyses. Here we revisit the torque formula and update many of its dimensionless coefficients by means of tailored, three-dimensional numerical simulations. In particular, we derive the dependence of the Lindblad torque on the temperature gradient, the dependence of the corotation torque on the radial entropy gradient (and work out a suitable expression of this gradient in a three-dimensional disc). We also work out the dependence of the corotation torque on the radial temperature gradient, overlooked so far. Corotation torques are known to scale very steeply with the width of the horseshoe region. We extend the expression of this width to the domain of intermediate mass planets, so that our updated torque formula remains valid for planets up to typically several tens of Earth masses, provided these relatively massive planets do not significantly deplete their coorbital region. Our torque expression can be applied to low- and intermediate-mass planets in optically thick protoplanetary discs, as well as protomoons embedded in circumplanetary discs.

Key words: Planetary systems: formation – Planetary systems: protoplanetary discs – Accretion, accretion discs – Methods: numerical – Hydrodynamics – Planet-disc interactions

1 INTRODUCTION

An important ingredient for studies of planetary population synthesis are the so-called migration maps, which are two-dimensional functions $\Gamma(M_p, r)$ that provide the torque exerted by the disc on a planet on a nearly circular orbit, as a function of its mass M_p and of its distance r to the central star. A migration map is intrinsic to a given disc model. Over most of the (M_p, r) domain, the torque is generally a negative quantity, corresponding to an orbital decay of the planet. Nevertheless, there may be some regions where the torque is positive (named islands of outward migration). These regions broadly occur where the disc’s temperature drops faster than r^{-1} , and span a mass range from a few Earth masses to potentially several tens of Earth masses. The outcomes of models of planet population synthesis depend sensitively on the outline of these islands (e.g. [Cossou et al. 2014](#)). Migration maps can be established in one of two

ways: they can either be obtained by three dimensional (3D) simulations, including all the physical ingredients needed for a correct description of the disc (e.g. [Lega et al. 2015](#)), or they can be obtained using torque formulae. The first approach is naturally not suitable to the exploration of a large number of disc models, owing to its considerable computational cost, and one must resort to torque formulae ([Masset & Casoli 2010](#); [Paardekooper et al. 2011](#)). Numerical simulations of low-mass planets embedded in radiative discs allows to assess the validity of torque formulae. [Bitsch & Kley \(2010\)](#) have compared the torque experienced by a $20 M_{\oplus}$ planet in a radiative disc to the predictions of [Paardekooper et al. \(2011\)](#) and [Masset & Casoli \(2010\)](#). The former displays a broad agreement with the outcome of the simulations. The latter, however, was found to be at odds with the simulations outcome, a discrepancy identified as too saturated corotation torques, and later resolved when estimates of the width of the horseshoe region in 3D discs became available ([Masset & Benítez-Llambay 2016](#)). Despite their broad agreement with simulation outcomes, the torque for-

[★] E-mail: mjimenez@icf.unam.mx

mulae of [Paardekooper et al. \(2011\)](#) and [Masset & Casoli \(2010\)](#) lack the accuracy required by models of planetary population synthesis. One of the main reasons is that these analyses are based on results of two-dimensional analysis. Even though they capture most of the mechanisms that contribute to the torque, the dimensionless coefficient that they feature in many places may be significantly off.

The purpose of this paper is to update the torque formula of [Masset & Casoli \(2010\)](#) by means of 3D numerical simulations, successively tailored to determine the value of each of the different dimensionless coefficients that we want to update. It is organised as follows. In section 3 we introduce and discuss the different torque components that we want to update and we describe the numerical code and setups that we use for this purpose. In section 4 we present our different results, and provide an updated torque formula in section 5. For the convenience of the reader mainly interested in the formula, this section is self-contained. We compare the results of our updated torque formula to published numerical simulations in section 6, and draw our conclusions in section 7.

2 NOTATION

We consider a planet of mass M_p on a circular orbit of radius r_p around a central star of mass M_\star , with angular speed Ω_p , embedded in a disc of surface density $\Sigma(r)$ which follows the power law:

$$\Sigma(r) = \Sigma_0 \left(\frac{r}{r_p} \right)^{-\alpha}. \quad (1)$$

The disc's midplane temperature $T(r)$ obeys the law:

$$T(r) = T_0 \left(\frac{r}{r_p} \right)^{-\beta}. \quad (2)$$

We denote with ν the kinematic viscosity of the disc, with χ its thermal diffusivity and with κ its opacity. The disc's pressure scale length is H , and is given by:

$$H = \frac{c_s}{\Omega_p}, \quad (3)$$

where c_s is the disc's isothermal sound speed:

$$c_s = \sqrt{\frac{\mathcal{R}T}{\mu}}, \quad (4)$$

\mathcal{R} being the constant of ideal gases and μ the mean molecular weight. We will also make use of the disc's aspect ratio

$$h = \frac{H}{r}, \quad (5)$$

and of the planet-to-star mass ratio

$$q = \frac{M_p}{M_\star}. \quad (6)$$

3 FOCUS OF OUR TORQUE UPDATE

Both the Lindblad and corotation torques can be normalised to:

$$\Gamma_0 = \Sigma_0 \Omega_p^2 r_p^4 \left(\frac{q}{h} \right)^2 = \Sigma_0 \Omega_p^4 r_p^6 q^2 c_s^{-2}. \quad (7)$$

We draw hereafter a list of the different updates that we perform on the normalised torques, which are dimensionless quantities.

3.1 Lindblad torque

The normalised Lindblad torque depends on α and β , which are respectively the slopes of surface density and temperature ([Ward 1986](#); [Korycansky & Pollack 1993](#)). Its dependence on α has already been worked out by [Tanaka et al. \(2002\)](#) by means of semi-analytical calculations in the linear regime for planets in globally isothermal discs, and we do not revise here this (weak) dependence. On the contrary, its dependence on the temperature slope has been worked out by [Paardekooper & Papaloizou \(2009a\)](#) by a linear analysis in two-dimensional discs with a softened potential.

Here we reevaluate the dependence of the Lindblad torque on the gradient of midplane temperature. We undertake this analysis in section 4.1. We note that the Lindblad torque can exhibit a dependence not only on α and β , but also on $\alpha\beta$ ([Korycansky & Pollack 1993](#)). This dependence is very weak, however, and we neglect it. More generally, we seek, and restrict ourselves to, linear dependencies of the different torque components on the radial gradients of physical quantities at the planet's location.

The Lindblad torque scales with the inverse squared of the sound speed (see Eq. 7). It therefore depends on the thermal diffusivity of the disc: when the latter is large enough that the disturbances triggered by the planet at Lindblad resonances behave isothermally, it scales with the inverse squared of the isothermal sound speed. On the other hand, when the thermal diffusivity is small and the disturbances behave adiabatically, the Lindblad torque scales with the inverse squared of the adiabatic sound speed, and is therefore a factor of γ smaller, where γ is the disc's adiabatic index. This dependence has been considered by [Masset & Casoli \(2010\)](#) and [Paardekooper et al. \(2011\)](#). We do not revise it here, and we will adopt for the updated expression of the Lindblad torque (see section 5.1) the dependence given by [Masset & Casoli \(2010\)](#).

3.2 Corotation torque

The corotation torque is the sum of three main components: one which scales with the radial gradient of vortensity, one which scales with the radial gradient of entropy, and one which scales with the radial gradient of temperature. In addition, there is a contribution to this torque arising from the vortensity viscously created at the contact discontinuities which appear on the downstream separatrices in the presence of an entropy gradient. These four contributions are represented in Fig. 1. Each of the first three components is a blend of a linear component and of a horseshoe drag. Each horseshoe drag is itself the product of the *unsaturated horseshoe drag* by a saturation function which is generally a number between 0 and 1 (corresponding respectively to a totally saturated and to an unsaturated horseshoe drag). Each torque component can in principle have its own saturation function.

We neither update, in this work, the saturation functions nor the blending coefficients. [Masset & Casoli \(2010\)](#)

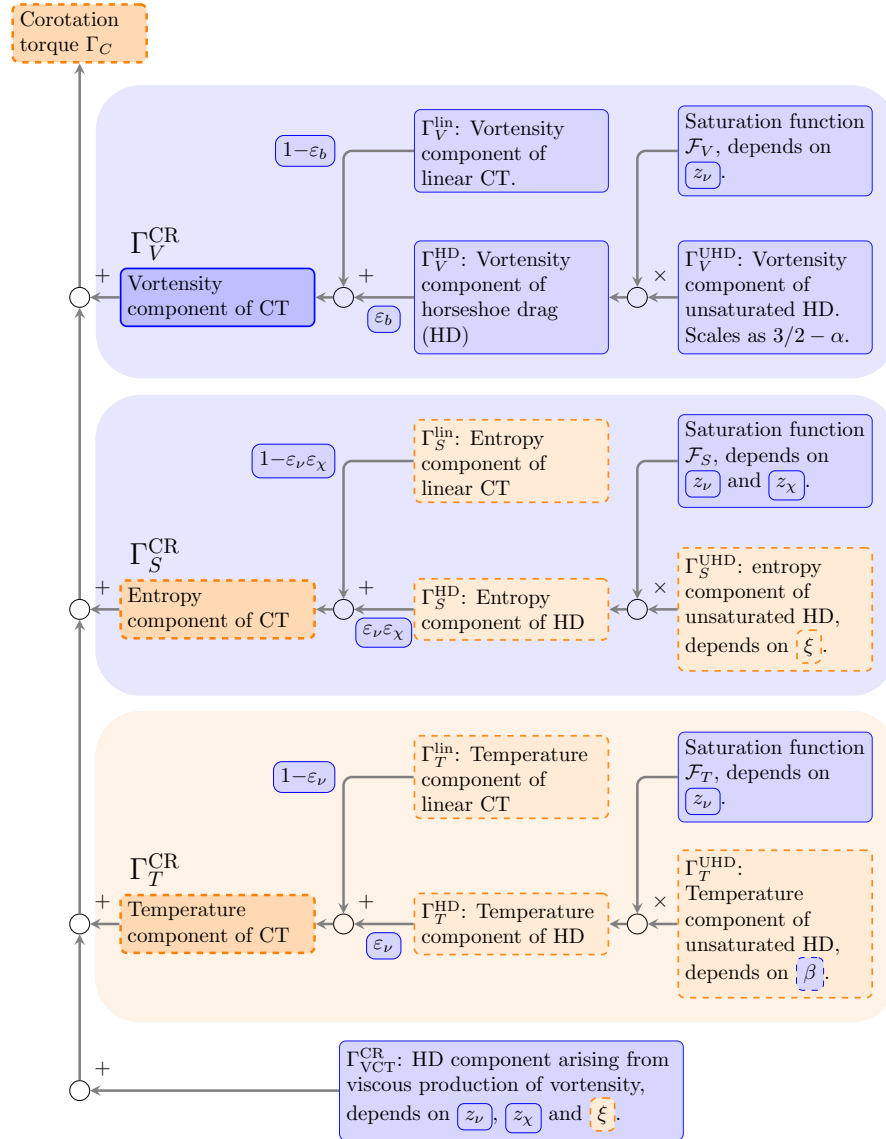


Figure 1. Synthetic representation of the different components of the corotation torque, showing how each of them is obtained (see section 3.2 for details). The blue rectangles show the components or variables which are not updated in this work. The orange rectangles (with a dashed frame to identify them on the printed version) show the variables or components for which we provide an updated version in this work. The component depending on the temperature gradient is integrated in a general torque formula for the first time, hence the orange background for this component. The weights ε_b , $1 - \varepsilon_b$, etc. displayed next to the arrows of the linear torques and horseshoe drags are the blending coefficients of these components. Their expression, as the expression of z_ν and z_χ , will be given in section 5. In the second frame (entropy torque), ξ represents the new expression of the entropy gradient.

gave an expression of the former, obtained from first principles by a two-dimensional analysis of a simplified model of the horseshoe flow. The horseshoe flow has since been shown to be essentially two-dimensional even in 3D discs (Masset & Benítez-Llambay 2016). On another hand, the flow arising from turbulence in three dimensions and that arising from a kinematic viscosity in a laminar 3D disc are markedly different (Fromang et al. 2011), so a 3D study of the torque saturation as a function of kinematic viscosity would probably be pushing the viscous model of protoplanetary discs beyond its domain of validity.

The blending coefficients were determined through a fit of numerical experiments by Masset & Casoli (2010) and by

Paardekooper et al. (2011). Masset & Casoli (2010) use the weights ε and $1 - \varepsilon$ respectively for the horseshoe drag and for the linear corotation torque (where ε depends on the torque component). Paardekooper et al. (2011) use the weights $1 - K$ and G , so that their sum is not necessarily 100%. This allows them to reproduce the fact that the horseshoe drag may be larger than its unsaturated value. In the analysis of Masset & Casoli (2010), this fact is incorporated at a different place (namely the fact that the saturation functions can have values slightly larger than unity). Here we stick to the blending coefficients of Masset & Casoli (2010).

The vortensity component of the corotation torque does not need any update. Masset & Benítez-Llambay (2016)

have shown that the 3D horseshoe drag in a barotropic disc has the same expression in a two dimensional disc, and that the horseshoe region has a vertical separatrix, hence a constant width on the whole vertical extent of the disc (see also [Fung et al. 2015](#)). Naturally, an updated width of the horseshoe region is used to evaluate this torque (more detail on this is given in section 4.4), but no amendment has to be done to the horseshoe drag expression. For the sake of simplicity, we consider here that the gradient of vortensity¹ is equal to $3/2 - \alpha$. This is true in any part of the disc where the surface density and angular frequency are power laws of the distance to the star.

The temperature component of the corotation torque has been overlooked in previous torque formulae. Here we obtain the value of this torque as a by-product of the study of the Lindblad torque of section 4.1 and present its properties in section 4.2. This torque component arises from the production of vortensity by the radial temperature gradient, and appears in locally isothermal calculations. The vortensity thus produced is concentrated near the (downstream) separatrices. Although it is not singular as the vortensity arising from non-barotropic effects, which can formally be represented by a delta-function at the separatrix ([Masset & Casoli 2009](#); [Paardekooper et al. 2010](#)), it has nearly same spatial distribution and it is reasonable to expect it to saturate in a similar manner. We therefore assume that this torque has same dependence on the viscosity as the entropy torque, and focus here exclusively on the magnitude of the unsaturated horseshoe drag and that of the linear torque.

Finally, we reevaluate the dependence of the entropy component on the entropy gradient, a much needed determination since this component plays a preponderant role in the appearance of outward migration islands in migration maps. We also reevaluate how to determine the entropy gradient in 3D disc. Whereas its expression is straightforward in 2D discs, one may contemplate different ways of evaluating it in a 3D disc (such as the gradient in the midplane, or of the vertically averaged quantity, etc.). Here we simply adopt the expression that yields to a one-to-one relationship (with the least possible dispersion) of the torque excess in a non-barotropic simulation with respect to a barotropic simulation. This analysis is presented in section 4.3.

3.3 Additional analysis

In addition to the aforementioned reevaluations of key dependencies of the torque, we have performed two side studies in order to improve the accuracy and predictive power of the torque formula, which we present below.

3.3.1 Width of horseshoe region

The different components of the horseshoe drag scale with the width of the horseshoe region to the fourth power. It is therefore crucial to get an accurate estimate of this width. Besides, as soon as the ratio q/h^3 is larger than ~ 0.1 , the law that gives the width for small mass planets ([Masset et al.](#)

[2006](#); [Paardekooper & Papaloizou 2009b](#); [Masset & Benítez-Llambay 2016](#)) is no longer valid and the horseshoe region is actually larger than what is predicted by the low-mass law, resulting in a boost of the corotation torque ([Masset et al. 2006](#); [Paardekooper & Papaloizou 2009b](#); [Duffell 2015](#)). The threshold of 0.1 is particularly stringent for typical protoplanetary discs, and translates into $4 M_{\oplus}$ only for a disc with an aspect ratio of $h = 0.05$ (which shows, incidentally, that the comparisons mentioned in section 1 were performed much beyond the domain of validity of the torque formulae for low-mass planets). In order to relax such a stringent condition on the planetary mass, we study here the transition between the low-mass regime, for which the width scales as $(q/h)^{1/2}$, and the high-mass regime, for which, as in the restricted three body problem, the width scales as $q^{1/3}$. This study is presented in section 4.4.

3.3.2 Thermal diffusivity

Since the saturation of the corotation torque depends on the value of the disc's thermal diffusivity, it is important to determine this value as accurately as possible. We have studied the radial spread of an initially localised excess of temperature in order to assess the accuracy of standard estimates which relate the disc's thermal diffusivity to the disc's temperature, density and opacity. This study is presented in section 4.5.

3.4 Numerical details

We conduct all our numerical experiments with the public hydrocode FARGO3D² ([Benítez-Llambay & Masset 2016](#)) with orbital advection enabled ([Masset 2000](#)). Here we use a spherical mesh that covers the full azimuthal range $[-\pi, \pi]$. We denote N_{ϕ} the number of cells in azimuth, N_r the number of cells in radius and N_{θ} the number of cells in colatitude. We always simulate a half-disc in colatitude (since the planet is always coplanar with the disc), and use reflecting boundary conditions at the midplane. All our calculations involving a planet are performed in the corotating frame.

According to our needs, we either use a locally isothermal equation of state, or we solve an energy equation. For the first case we use the closure relationship between the pressure p and density ρ :

$$p(\mathbf{r}, t) = c_s^2(r)\rho(\mathbf{r}, t), \quad (8)$$

where $c_s(r)$ is the isothermal sound speed, which depends on the distance to the central star, and which is constant in time. In such case there is no need to solve an energy equation. In the second case, we solve the time evolution of the internal equation, and in the absence of some form of thermal diffusion, the flow behaves adiabatically. In this case we assume the gas to be ideal, so that the pressure is given by:

$$p(\mathbf{r}, t) = (\gamma - 1)e(\mathbf{r}, t), \quad (9)$$

where e is the internal energy density.

Finally, in order to avoid the divergence of the planetary

¹ More specifically, the quantity $d \log(\Sigma/B)/d \log r$, where B , the second Oort's constant, is half the flow's vertical vorticity.

² <http://fargo.in2p3.fr>

potential Φ_p in the vicinity of the planet, we soften it over a length scale ϵ :

$$\Phi_p(\mathbf{r}) = -\frac{GM_p}{\sqrt{|\mathbf{r} - \mathbf{r}_p|^2 + \epsilon^2}}. \quad (10)$$

In three-dimensional calculations, ϵ has to be chosen small compared to the pressure scale length, and larger or comparable to the resolution. In all our numerical experiments we have $\epsilon = 0.1H$.

4 RESULTS

We present hereafter the results of the numerical experiments conducted to address the points listed in section 3.

4.1 Dependence of the Lindblad torque on the temperature gradient

For this experiment, we use a locally isothermal setup, and use the fact that at larger time the corotation torque saturates, so that the total torque essentially amounts to the Lindblad torque.

In a locally isothermal setup, the Lindblad torque has the form:

$$\frac{\Gamma_L}{\Gamma_0} = -(2.34 - 0.099\alpha + k\beta), \quad (11)$$

where as discussed in section 3.1 the first two terms of the right hand side come from the work of Tanaka et al. (2002), and where k is the coefficient that we want to determine. In principle, it suffices to perform two runs which have different values of β (all other parameters being the same) to infer k .

Our choice of parameters results from a trade-off between different effects. We want the planetary mass to be sufficiently large so that the horseshoe region is well resolved and can be saturated in a reasonable amount of time. On the other hand, we want the planetary mass to be sufficiently small so that the planet does not significantly perturb the disc by carving a gap.

There is another difficulty inherent to this experiment: when the disc is not globally isothermal ($\beta \neq 0$), it is prone to a baroclinic instability (Klahr 2004) which results in considerable noise in the torque curves, precluding any converged measurement. However interesting this instability may be, it has for us a parasitic character, and we aim at getting rid of it, while preserving an almost complete saturation of the corotation torque. We prevent the appearance of the instability by using some amount of viscosity, and determine by dichotomy the minimal amount of viscosity required to quench the instability. Also, the strength of the instability scales with $|\beta|$, so one has to choose values of β sufficiently large to allow an accurate measurement of k , but also sufficiently small to avoid the development of the baroclinic instability, once the viscosity has been chosen.

With these considerations in mind, we have chosen for this numerical experiment the following values: $q = 2.4 \cdot 10^{-5}$ (which corresponds to $8 M_\oplus$ if the central star has a solar mass) and $\nu = 7 \cdot 10^{-8} r_p^2 \Omega_p$. The disc's aspect ratio is $h = 0.05$. Although the kinematic viscosity is quite small, we do not expect the planet to carve a significant gap in

the disc over the time scale required to achieve the saturation of the corotation torque. The Hill radius of the planet [$r_p(q/3)^{1/3}$] is much smaller than the pressure length scale, and the expression $3h/[4(q/3)^{1/3}] + 50\nu/(r_p^2 \Omega_p q)$ is a factor of 2 above the critical value for gap opening (see Eq. (15) of Crida et al. 2006). Even under these conditions a gap may eventually be opened (Dong et al. 2011; Fung et al. 2014; Kanagawa et al. 2015), but this will occur on time scales much longer than those of our numerical experiments. As we shall see below, we do find evidence for secular effects in our torque measurements, which affect our results at the percent level.

Our mesh extends from $\pi/2 - 3h$ to $\pi/2$ in colatitude, over $N_\theta = 40$ cells, and from $0.6r_p$ to $1.4r_p$ in radius, over $N_r = 200$ cells. In addition, we have $N_\phi = 900$ cells. We use wave-killing boundary conditions in radius (de Val-Borro et al. 2006), in order to avoid reflection of the wake at the radial boundaries. We therefore expect our results to be nearly insensitive to the exact location of the mesh radial boundaries, as these are located at a large number of pressure scale lengths from the orbit. We perform two simulations, with $\beta = 1/2$ and $\beta = -1/2$ respectively. Each one is run over 1000 orbital periods of the planet. We choose $\alpha = 3/2$ so that there is no vortensity gradient, and the only corotation torque present before saturation is the temperature component of the corotation torque.

This choice of parameters implies that the horseshoe region is resolved over 11 zones, which is sufficient to allow for a nearly complete saturation of the torque (Masset & Ogilvie 2004). We have $q/h^3 = 0.19$, so that the flow is weakly non-linear. The horseshoe libration time is ~ 60 orbits, so that our runs duration allows for a full saturation of the corotation torque. The ratio of the viscous time scale across the horseshoe region to the libration time scale is ~ 7 , which implies that the corotation should reach a degree of saturation of $\sim 90\%$. We show the torque as a function of time for the two runs in Fig. 2. The corotation torque saturates, leaving essentially the Lindblad torque. We see a systematic, slow increase of the torque in both cases, which we attribute to the slow opening of a very shallow dip (we find that the rate of this increase decays as the viscosity increases).

The value of k can be directly obtained by subtracting the two normalised torques. We show their difference in Fig. 3. From this figure we infer a value of $k \approx 1.4$, comparable to, and marginally smaller than the value of 1.7 found by Paardekooper & Papaloizou (2009a) for 2D discs.

4.2 Dependence of the corotation torque on the temperature gradient

We can further exploit the runs presented at the previous section to work out the dependence on β of Γ_T^{UHD} and Γ_T^{lin} (see Fig. 1). Over the first half libration time, the torque is the sum of the Lindblad torque and the unsaturated horseshoe drag. Since there is no vortensity gradient in these runs, the horseshoe drag is entirely attributable to the temperature gradient. As we now have an expression of the Lindblad torque that takes the temperature gradient into account, we can subtract this torque from the torque measured to get an estimate of the corotation torque. We can also slightly improve upon the results of the previous section by taking into

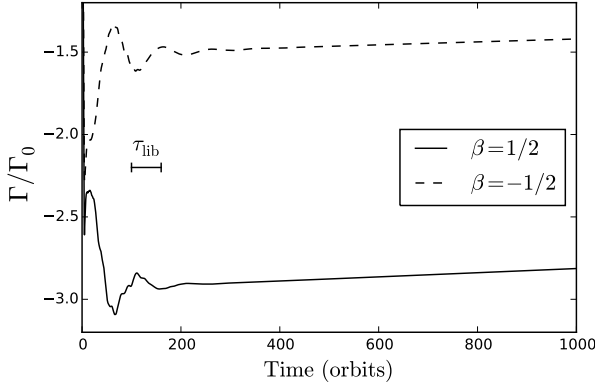


Figure 2. Total normalised torque on a planet with $q = 2.4 \cdot 10^{-5}$ for two different values of β , in a locally isothermal disc. The horizontal segment near 100 orbits shows the horseshoe libration time. Past ~ 300 orbits, the corotation torque has saturated and the torque essentially amounts to the Lindblad torque. We see a systematic increase of the normalised torque of about ~ 0.2 , in both cases, over 1000 orbits.

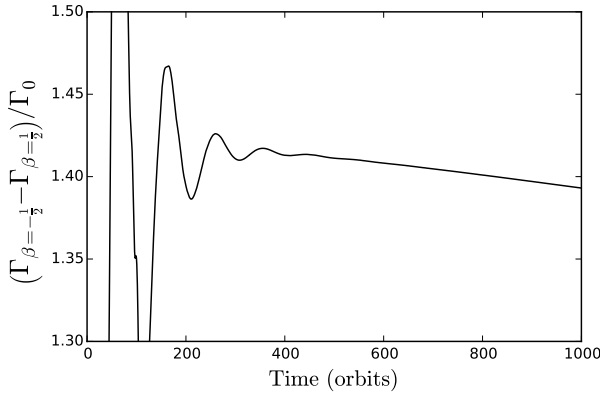


Figure 3. Result of the subtraction of the two curves of Fig. 2. The rising trends of the torques largely cancel out, and the difference shows an overall variation at the percent level.

account the residual value of the corotation torque at larger time, as it does not fully saturate. We write the torque over the first half libration time as:

$$\Gamma_{\beta}^{(U)} = \Gamma_L + \Gamma_T^{\text{UHD}}, \quad (12)$$

where the (U) superscript stands for “unsaturated”, and where the β subscript conveys that in this numerical experiment the only parameter that is varied is β . In Eq. (12), we do not have a vortensity component for the reasons exposed above, and we do not have an entropy component either because the setup is isothermal. The planetary mass is sufficiently large, and the viscosity sufficiently small, for the torque to be the (unsaturated) horseshoe drag (Paardekooper & Papaloizou 2009a).

Writing the unsaturated corotation torque as

$$\Gamma_T^{\text{UHD}} = k' \beta \Gamma_0, \quad (13)$$

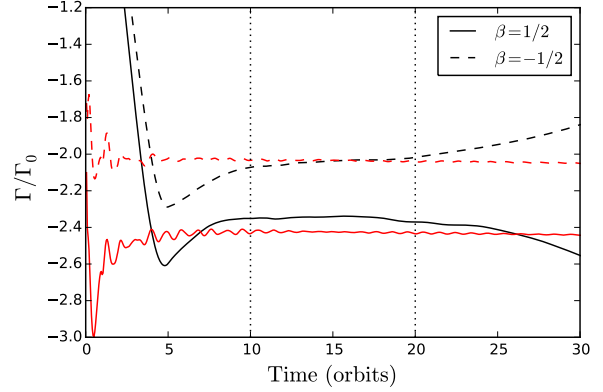


Figure 4. Torque as a function of time over the first half libration time, for the two runs presented in section 4.1 (black curves). The torques reach a plateau after ~ 10 orbits, and begin to depart from this plateau around ~ 20 orbits. The time averaged values between 10 and 20 orbits is $-2.34\Gamma_0$ for $\beta = 1/2$ and $-2.04\Gamma_0$ for $\beta = -1/2$. The grey curves (red in the electronic version) show the normalised torques for the same parameters, except that $q = 3 \cdot 10^{-6}$ and $\nu = 10^{-5} r_p^2 \Omega_p$, so that the corotation torque remains linear.

where k' is the dimensionless coefficient that we want to determine, we can write:

$$\frac{\Gamma_{\beta}^{(U)}}{\Gamma_0} = K - k\beta + k'\beta, \quad (14)$$

where $K = -2.34 + 0.099\alpha$ (Tanaka et al. 2002). We can also write the torque value at larger time as

$$\frac{\Gamma_{\beta}^{\infty}}{\Gamma_0} = K - k\beta + \epsilon k'\beta, \quad (15)$$

where $\epsilon \ll 1$ represents the amount of saturation of the corotation torque. From these relations we infer:

$$k - \epsilon k' = \frac{\Gamma_{-1/2}^{\infty} - \Gamma_{1/2}^{\infty}}{\Gamma_0} \equiv \frac{\Delta\Gamma^{\infty}}{\Gamma_0} \quad (16)$$

$$k - k' = \frac{\Gamma_{-1/2}^{(U)} - \Gamma_{1/2}^{(U)}}{\Gamma_0} \equiv \frac{\Delta\Gamma^{(U)}}{\Gamma_0}, \quad (17)$$

hence

$$k = \frac{\Delta\Gamma^{\infty} - \epsilon\Delta\Gamma^{(U)}}{\Gamma_0(1 - \epsilon)} \quad (18)$$

$$k' = \frac{\Delta\Gamma^{\infty} - \Delta\Gamma^{(U)}}{\Gamma_0(1 - \epsilon)}. \quad (19)$$

We recover the fact that $k = \Delta\Gamma^{\infty}/\Gamma_0$ when $\epsilon = 0$, that is to say when the corotation torque is fully saturated at larger time. Fig. 4 shows the torque behaviour at early time, from which we infer $\Delta\Gamma^{(U)} = 0.3\Gamma_0$. When $\epsilon = 0$, this yields $k' = 1.1$. Evaluating k and k' when $\epsilon = 0.1$ (a reasonable amount of residual corotation torque, as discussed in section 4.1), we get $k = 1.5$, and $k' = 1.2$. This shows that the coefficients that we have obtained for the temperature dependence of the normalised Lindblad and corotation torques are accurate to within ~ 0.1 .

We conclude this section by determining in a similar

manner the linear corotation torque. We simply have to amend the parameters so that the corotation torque remains linear. This is achieved by adopting a much smaller planet mass and a large viscosity (Paardekooper & Papaloizou 2009a). The results of these new runs are displayed in Fig. 4, in which one can see that indeed the torques remain nearly constant after a dynamical timescale and do not show the variation toward a different value on $O(10)$ orbits typical of the horseshoe drag (Paardekooper & Papaloizou 2009a). These results imply that the temperature component of the linear corotation torque scales as:

$$\Gamma_T^{\text{lin}} = 1.0\beta\Gamma_0, \quad (20)$$

where again the numerical coefficient is determined to within ~ 0.1 . At this stage, considering that we use the saturation function and the weights provided by Masset & Casoli (2010), we have completed our determination of the terms entering in Γ_T^{CR} (see Fig. 1, third frame).

4.3 Torque dependence on the radial entropy gradient

We now perform a 3D version of the study presented by Baruteau & Masset (2013) and update the terms entering in Γ_S^{CR} (see Fig. 1, second frame). We take an adiabatic index $\gamma = 1.4$, unless stated otherwise. We consider a large number of disc models (here $N = 80$) for which each value of the surface density and temperature slopes are chosen randomly (namely, α is given by a random variable uniformly distributed over $[-1.5, 1.5]$, while β is uniformly distributed over $[-2, 2]$). For each disc model, two runs are performed: one with a locally isothermal equation of state, and one with an adiabatic flow, which provide respectively the torque Γ_{iso} and Γ_{adi} . The parameters and the duration of the runs are such that the corotation torque is in the regime of unsaturated horseshoe drag. We then seek an appropriate linear combination ξ of α and β such that the torque excess, defined as $\Delta\Gamma = \gamma\Gamma_{\text{adi}} - \Gamma_{\text{iso}}$, be a one-to-one map of ξ . We illustrate this process in Fig. 5. We find that an appropriate expression for ξ is the following:

$$\xi = \beta - 0.4\alpha - 0.64, \quad (21)$$

and that in this case we have:

$$\Delta\Gamma = 4.6\xi\Gamma_0. \quad (22)$$

By construction, our procedure implies that there is a linear relationship between ξ and the torque excess, and therefore the calculation of the adiabatic torque is straightforward once one knows the isothermal torque. In a 2D situation, the excess has been found to scale with the radial entropy gradient (Baruteau & Masset 2008; Paardekooper & Papaloizou 2008; Masset & Casoli 2009). Here, its expression resembles the gradient of entropy evaluated in the midplane³, which is $\beta - 2(\gamma - 1)/(3 - \gamma)\alpha - 3(\gamma - 1)/(3 - \gamma) = \beta - 0.5\alpha - 0.75$, but differs slightly from it. By extension, we call ξ the radial entropy gradient, but it must be kept in mind that this is an abuse of language, as this quantity has not been obtained by considerations about the entropy,

³ Here this gradient is normalised so that the coefficient of β is one.

but by a fit of numerical simulations. As mentioned in section 3.2, we assume that this corotation torque component saturates as the entropy-related torque in 2D discs.

We have not investigated in a systematic manner the dependency of the different coefficients of Eq. (21) on the adiabatic index. Nonetheless, for the reader interested in the torque in a different kind of discs, we mentioned that we have conducted a similar study for the case $\gamma = 5/3$, and found in that case that $\xi = \beta - 0.58\alpha - 0.85$ provides the one-to-one linear relationship $\Delta\Gamma = 4.1\xi\Gamma_0$.

At this stage we see that the horseshoe drag in the adiabatic case is the sum of a term that scales with ξ (combination of α and β) and of the isothermal horseshoe drag, itself sum of a term that scales with the vortensity gradient ($\frac{3}{2} - \alpha$ in power law discs) and a term that scales with the temperature gradient (β) as found in section 4.2. We have three components and only two slopes (α and β). It may seem desirable at first glance to simplify the expression for the net corotation torque into a dependence on α and one on β . This, as discussed by Baruteau & Masset (2013), would obfuscate the physical meaning of each term. Besides, each component involves a different distribution of vortensity perturbation within the horseshoe region, and thus in principle saturates in a different manner, so the simplification could only be valid for the regime of unsaturated horseshoe drag, not for the general regime. We shall therefore keep the three components in the general expression of the corotation torque.

We have performed a numerical experiment similar to the one described above, with a lower mass ($q = 10^{-6}$) and a higher viscosity ($\nu = 2 \cdot 10^{-5} r_p^2 \Omega_p$), so that the corotation torque remains linear (Paardekooper & Papaloizou 2009a). We find in that case:

$$\Delta\Gamma^{\text{lin}} = 0.8\xi\Gamma_0. \quad (23)$$

4.4 Width of the horseshoe region

As said in section 3.3.1, the different components of the horseshoe drag scale with the width of the horseshoe region to the fourth power. It is therefore important to have an accurate value of this width, so we study its scaling as a function of the planet mass in the regimes of low and intermediate masses, corresponding respectively to $q \ll h^3$ and $q \lesssim h^3$ (we shall provide slightly more quantitative definitions at the end of this section). For this purpose we use globally isothermal simulations, and perform a streamline analysis in the midplane, exploiting the fact that the horseshoe region has a width which is independent of the altitude in this case (Fung et al. 2015; Masset & Benítez-Llambay 2016). Our runs have a setup similar to the setup outlined in section 4.1, except for the resolution $(N_\phi, N_r, N_\theta) = (1320, 440, 40)$. In particular, we still have a null vortensity gradient. Casoli & Masset (2009) have found that the horseshoe region is asymmetric when the vortensity gradient is finite. Even though we average the width of the horseshoe region in front and at the rear of the planet in order to minimise the effect of an asymmetry, we prefer not to introduce a source of asymmetry of the horseshoe region⁴. The planet mass is introduced

⁴ The result of Casoli & Masset (2009) was obtained in two-dimensional discs. No similar result has been obtained in three-

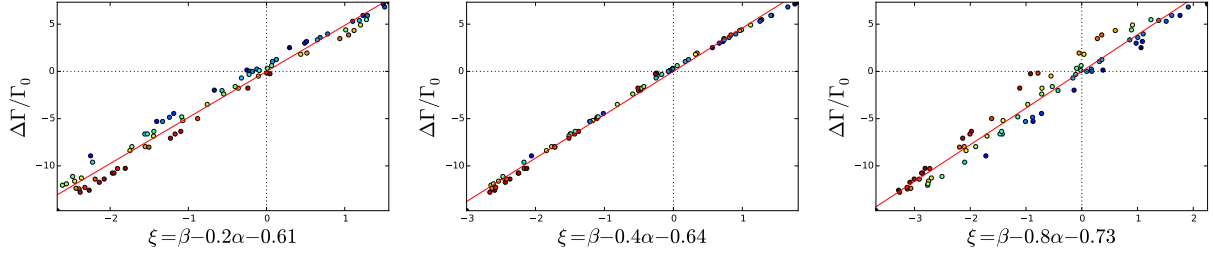


Figure 5. Torque difference $\Delta\Gamma$ between an adiabatic and isothermal setup, as a function of ξ , linear combination of β and α . We keep the coefficient of β at the fixed value of one, and search the coefficient of α that minimises the sum of the squared distances to a linear fit. The first and third plots show cases for which a large scatter subsists, while the middle plot corresponds to the smallest sum of distances to the fit (solid line), hence to the best adjustment. In addition, we add a constant value to ξ so that the linear fit of the data has no constant term, resulting in $\Delta\Gamma$ being proportional to ξ . In the electronic version, the points are coloured from blue to red according to the value of α (blue corresponds to -1.5 and red to 1.5).

progressively over two orbital periods, and the width of the horseshoe region is measured 20 orbits after the introduction of the planet. We perform a systematic study for three values of the aspect ratio: $h = 0.03$, $h = 0.04$ and $h = 0.05$. For each of these values, we perform 30 calculations with a planetary mass varying in a geometric sequence from $0.05h^3$ to $4h^3$. The width of the horseshoe region is determined automatically by dichotomy, averaging the results in $\phi = 1$ rad and $\phi = -1$ rad. We find that more accurate results are obtained if the disc is inviscid when $q < 0.4h^3$, and viscous for larger masses. For lower mass indeed, a viscous drift of the disc can distort severely the horseshoe region (Masset 2002), whereas for high masses, the planet can trigger vortices on the edges of its horseshoe region if the disc is inviscid, which precludes an accurate determination of the width of the horseshoe region.

For low masses, we have the scaling (Lega et al. 2015; Masset & Benítez-Llambay 2016):

$$x_s = 1.05r_p \sqrt{\frac{q}{h}}, \quad (24)$$

whereas for large masses we recover the scaling found in 2D simulation with softened potential (Masset et al. 2006):

$$x_s \approx 2.5r_p (q/3)^{1/3}. \quad (25)$$

Using the width normalised to the pressure length scale $X_s = x_s/(hr_p)$ and denoting with Q the planetary mass normalised to the thermal mass $M_{\text{th}} = c_s^3/(G\Omega_p)$:

$$Q = \frac{M_p}{M_{\text{th}}} = \frac{q}{h^3}, \quad (26)$$

we can rewrite Eqs. (24) and (25) as:

$$X_s = 1.05Q^{1/2} \quad \text{when } Q \ll 1 \quad (27)$$

and

$$X_s = 1.7Q^{1/3} \quad \text{when } Q \gg 1. \quad (28)$$

The lack of an explicit reference to h in these expressions suggests that the normalised width of the horseshoe region has a universal dependence on the mass expressed in thermal masses. Fig. 6 confirms this expectation. We find that

dimensional discs, so we assume that adopting a null vortensity gradient keeps the degree of asymmetry to an acceptable level.

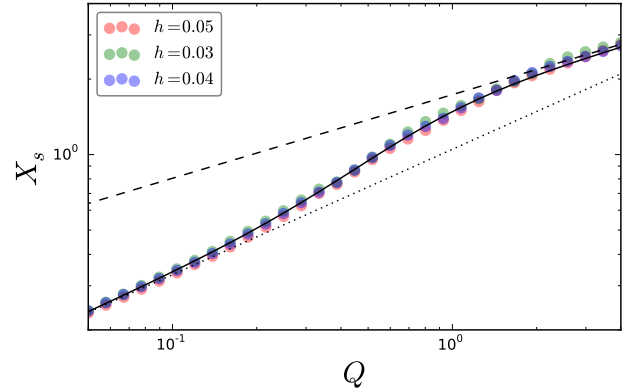


Figure 6. Normalised half width of the horseshoe region as a function of the mass in thermal masses. The data from the three different aspect ratios coincide nearly exactly. The solid curve corresponds to Eq. (29), the dotted curve to Eq. (27) and the dashed curve to Eq. (28). This figure should be compared to Fig. 7 of Lega et al. (2015).

a function that gives the asymptotic behaviours of Eq. (27) and (28) and that matches satisfactorily the width behaviour for intermediate masses is a blend of the asymptotic values at low- and large-mass with weights respectively ϵ and $1 - \epsilon$, where $\epsilon = 1/(1 + 2Q^2)$. This yields:

$$X_s = \frac{1.05Q^{1/2} + 3.4Q^{7/3}}{1 + 2Q^2}, \quad (29)$$

or

$$x_s = \frac{1.05(q/h)^{1/2} + 3.4q^{7/3}/h^6}{1 + 2q^2/h^6} r_p. \quad (30)$$

From now on we will use Eq. (30) to evaluate the width of the horseshoe region.

As a side result, this leads us to a reasonable definition of an *intermediate* mass protoplanet as a protoplanet that has a horseshoe width intermediate between the widths given by the low-mass and high-mass scaling (Eqs. (24) and (25)). Examination of Fig. 6 shows that this broadly corresponds to $0.2h^3 \lesssim q \lesssim 2h^3$.

We assume that the corotation torque tends toward its linear value when dissipation (either viscous or thermal)

is large, regardless of the planetary mass. This result has been shown by [Paardekooper & Papaloizou \(2009a\)](#) for low-mass planets, but it may be questionable for intermediate mass objects. Although we have not explored this issue in a systematic manner, we have performed simulations with a planet of half the thermal mass ($Q = 0.5$), and found that it is subjected, at very large viscosity, to a vortensity corotation torque comparable to the linear estimate. This result was obtained considering globally isothermal discs with and without vortensity gradients⁵. We note, however, that a substantial amount of dissipation is required for a fall back of the corotation torque of an intermediate mass object to its linear estimate. The decay toward the linear regime is obtained for (e.g. [Masset & Casoli 2010](#)):

$$\frac{hr_p \nu}{\Omega_p x_s^3} \gg 0.1, \quad (31)$$

and a similar condition holds, obtained by writing χ in stead of ν , for the decay of the entropy torque to its linear value. We introduce the disc's alpha parameter α_{ss} ([Shakura & Sunyaev 1973](#)), and write $\nu = \alpha_{ss} r_p^2 \Omega_p h^2$. Using for x_s the conservative value given by the low-mass estimate, we recast the condition of Eq. (31) as:

$$\alpha_{ss} \gg 0.1 Q^{3/2}. \quad (32)$$

For $Q = 0.2$, which corresponds to the mass at which departure from the small mass regime becomes noticeable, this translates into $\alpha_{ss} \gg 10^{-2}$. This implies that under most circumstances the corotation torque exerted on intermediate mass objects should essentially be the horseshoe drag.

4.5 Thermal diffusion coefficient

Previous estimates of the thermal diffusion coefficient have been obtained by using values at the midplane of the disc (e.g. [Paardekooper et al. 2011](#); [Bitsch & Kley 2011](#); [Bitsch et al. 2014](#)). We have undertaken simulations to check whether heat diffusion can indeed be described by a diffusion coefficient evaluated at the disc's midplane.

Following [Kley et al. \(2009\)](#), we write the thermal diffusivity, in the absence of scattering, as (their Eq. B.2):

$$\chi = \frac{D}{c_v \rho} = \lambda \frac{4acT^3}{\rho^2 c_v \kappa}, \quad (33)$$

where D is the heat diffusion coefficient, λ , the flux-limiter, is 1/3 in the optically thick regions where the planet is located, a is the radiation constant and c_v is the specific heat at constant volume. We can recast Eq. (33) as:

$$\chi = \frac{16(\gamma - 1)\sigma T^3}{3\rho^2(\mathcal{R}/\mu)\kappa}, \quad (34)$$

⁵ The unsaturated *total* torque in isothermal simulations when $Q \sim 0.5$ can be off by several Γ_0 from its expected value, whereas we found with subsidiary calculations of isentropic discs that the total torque is correctly reproduced. These different behaviours have also been observed by [Fung et al. \(2015, 2017\)](#) and are linked to small scale features of the flow. Since the realistic discs in which we apply our torque formula are not isothermal, we believe that this discrepancy is unimportant, but it should be kept in mind when dealing with intermediate mass planets embedded in isothermal discs.

where σ is Stefan's constant. We note that this expression has oftentimes been transformed into an expression involving the disc's thickness H and orbital frequency Ω at the denominator. These expressions, in general, overestimate by a factor γ the thermal diffusivity of Eq. (34). The equation that describes the hydrostatic equilibrium of the disc does not involve the adiabatic index, and it yields the relationship $H = c_s/\Omega$, rather than $H = c_s^{\text{adi}}/\Omega = \sqrt{\gamma}c_s/\Omega$, independently of the fact that an energy equation is used to describe the flow. However, we suggest to simply use Eq. (34) rather than the transformed expression, as the latter, which features all the variables of Eq. (34) as well as new ones, does not bring any simplification.

Here, we specifically study the *radial* diffusion of heat, as it is mainly this effect which determines (together with viscous diffusion) the degree of saturation of the horseshoe drag. Namely, we study the radial spread of a radially localised temperature excess in order to determine experimentally the thermal diffusivity of the disc and compare it to the theoretical estimate. In this section only we use a module of radiative transfer in the flux limited diffusion approximation ([Levermore & Pomraning 1981](#)) with the flux limiter of [Kley \(1989\)](#), and solve the equation of radiative energy in addition to that of internal energy (two-temperature approach) as in [Bitsch et al. \(2013\)](#). We use a meridional mesh of size $(N_\phi, N_r, N_\theta) = (1, 800, 43)$ spanning a radial range of 0.75 au to 3 au, and a range in colatitude $[\pi/2 - 0.1, \pi/2]$. The surface density at 1 au is $\Sigma_0 = 1700 \text{ g cm}^{-2}$, the Rosseland opacity is fixed to $1.8 \text{ cm}^2 \text{ g}^{-1}$, and the kinematic viscosity is $\nu = 4.46 \cdot 10^{14} \text{ cm}^2 \text{ s}^{-1}$. The slope of surface density is $\alpha = 0.3$. The temperature profile of the disc at equilibrium depends on a balance between viscous heating and radiative losses through the disc's photospheres. We firstly run our initial setup, which has an arbitrary aspect ratio, in order to relax the disc toward hydrostatic and thermal equilibria. Once these are reached, we increase by 1 % the temperature of a three-zone wide ring at $r = 1.5 \text{ au}$ (over the whole colatitude range), and restart the simulation (hot ring run). We also perform a "neutral" restart in which the temperature has not been altered. The radial profile of the temperature excess obtained by subtracting the temperature profile of the neutral run from the hot ring run (at the same date), quickly adopts a nearly Gaussian profile:

$$\delta T(r, t) \propto \frac{1}{\sigma(t)} \exp[-(r - r_0)^2 / \sigma^2(t)]. \quad (35)$$

In linear diffusion theory, $\sigma^2(t) = 4\chi t$. We use this relationship to infer the value of χ . Fig. 7 shows the time behaviour of σ^2 , which is nearly linear in time, as expected. From the slope of the linear regression fit, we can estimate that the value of χ at $r = r_0$ is:

$$\chi \approx 1.03 \cdot 10^{15} \text{ cm}^2 \text{ s}^{-1}. \quad (36)$$

An estimate based on the temperature excess averaged in colatitude, rather than measured at the midplane, yields nearly exactly the same result. At $r = 1.5 \text{ au}$, we have in the neutral run a midplane temperature $T = 509 \text{ K}$, a density $\rho = 4.33 \cdot 10^{-10} \text{ g cm}^{-3}$, and $\mathcal{R}/\mu = 3.615 \cdot 10^7 \text{ erg K}^{-1} \text{ g}^{-1}$. Eqs. (34) yields a value 27 % larger than the value found experimentally.

The disc of this numerical experiment is in radiative equilibrium and its only source of heating is viscous friction.

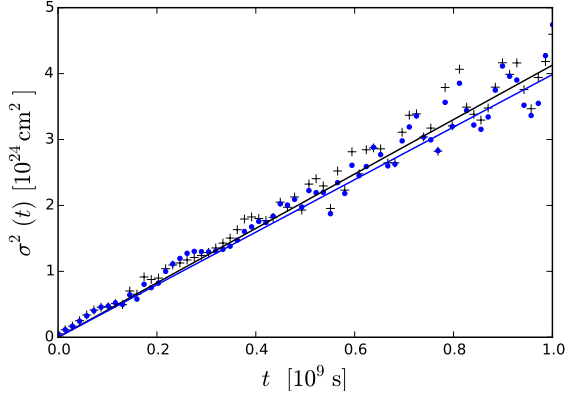


Figure 7. Mean square deviation of the temperature excess as a function of time. The crosses are obtained by a measure of the full width at half maximum (divided by $2\sqrt{\log 2}$) and the dots (in blue in the electronic version) are obtained by means of a second order polynomial fit of $\log \delta T$ on a 14-cell interval centred on $r_0 = 1.5$ au. The slope obtained by a linear regression fit of the crosses is $4.17 \cdot 10^{15} \text{ cm}^2 \text{ s}^{-1}$, whereas the slope obtained by a linear regression fit of the dots is $4.05 \cdot 10^{15} \text{ cm}^2 \text{ s}^{-1}$.

Its temperature therefore decays from the midplane to low values near the boundaries in colatitude. We have repeated this numerical experiment with a nearly isothermal vertical profile, obtained by lowering the viscosity by a factor of ten and by imposing a temperature at the upper boundary T_b such that $T_b^4 = 0.9T_{\text{midplane}}^4$. The vertical heat flux is therefore lowered by an order of magnitude with respect to the previous disc, the temperature is nearly constant with respect to colatitude, and the resulting disc has same midplane temperature as the previous one.

We measured a thermal diffusivity nearly equal to the one of the previous disc, which shows that this quantity is rather insensitive to the vertical profile of temperature, and determined by the midplane temperature.

5 NEW TORQUE FORMULA

We hereafter summarise our results and provide an updated torque formula for different cases: the general case, the linear regime for a radiative disc, and the linear regime for an isothermal disc.

5.1 General case

Usually torque expressions are given in terms of the reference torque Γ_0 of Eq. (7). For the horseshoe drag, this expression arises naturally when using the low mass value of the horseshoe width (Eq. 24), and an horseshoe drag expression, which involves the product $\Sigma_0 \Omega_p^2 x_s^4$. Here, however, we use a more complex law (Eq. 30) for the horseshoe width, so that casting our results in terms of Γ_0 , for the different components of the corotation torque, would lead to cumbersome expressions. We therefore rather cast the different components of the horseshoe drag in terms of x_s .

The total torque is a function of the slopes of surface

density and temperature α and β , of the disc's opacity, viscosity, aspect ratio and surface density (respectively κ , ν , h and Σ_0) and of the planet orbital frequency, orbital radius and mass to star mass ratio (respectively Ω_p , r_p and q). It requires the prior evaluation of the thermal diffusivity using Eq. (34), and that of the half width of the horseshoe region x_s , which is given, when the flow is adiabatic or behaves nearly adiabatically over the horseshoe U-turn timescale, by a modification of Eq. (30) that uses the adiabatic sound speed, rather than the isothermal one:

$$x_s = \frac{1.05(q/h')^{1/2} + 3.4q^{7/3}/h'^6}{1 + 2q^2/h'^6} r_p, \quad (37)$$

where $h' = h\sqrt{\gamma}$.

The total torque is the sum of the Lindblad torque Γ_L and corotation torque Γ_C :

$$\Gamma_{\text{tot}} = \Gamma_L + \Gamma_C. \quad (38)$$

The Lindblad torque is given by:

$$\Gamma_L = -(2.34 - 0.1\alpha + 1.5\beta)\Gamma_0 f(\chi/\chi_c), \quad (39)$$

where the first two coefficients in the factor of the right hand side (2.34 and -0.1) are given by Tanaka et al. (2002), and where an approximate value of the third coefficient (the factor of β) has been obtained in section 4.1 and subsequently slightly improved in section 4.2. The function $f(x)$ and critical diffusivity χ_c are given by Masset & Casoli (2010) and have respectively the expressions:

$$f(x) = \frac{(x/2)^{1/2} + 1/\gamma}{(x/2)^{1/2} + 1}, \quad (40)$$

and:

$$\chi_c = r_p^2 h^2 \Omega_p. \quad (41)$$

The function $f(\chi/\chi_c)$ can be regarded as the inverse of an effective adiabatic index γ_{eff} (see also Paardekooper et al. 2011).

We now turn to the evaluation of the four terms that compose the corotation torque (see Fig. 1). The vortensity component Γ_V^{CR} of the corotation torque is given by:

$$\Gamma_V^{\text{CR}} = \varepsilon_b \Gamma_V^{\text{HD}} + (1 - \varepsilon_b) \Gamma_V^{\text{lin}}. \quad (42)$$

In this expression, the blending coefficient ε_b , as advertised in section 3, has the expression worked out by Masset & Casoli (2010):

$$\varepsilon_b = (1 + 30hz_\nu)^{-1}, \quad (43)$$

where z_ν is given by Masset & Casoli (2010, Eq. 79):

$$z_\nu = \frac{r_p \nu}{\Omega_p x_s^3}. \quad (44)$$

The (vortensity components of the) horseshoe drag Γ_V^{HD} and linear corotation torque Γ_V^{lin} are respectively:

$$\Gamma_V^{\text{HD}} = \mathcal{F}_V \Gamma_V^{\text{UHD}}, \quad (45)$$

and

$$\Gamma_V^{\text{lin}} = (0.976 - 0.640\alpha)\Sigma_0 \Omega_p^2 r_p^4 (h')^{-2} = (0.976 - 0.640\alpha)\Gamma_0/\gamma, \quad (46)$$

where the numerical coefficients of the right hand side of

Eq. (46) can be obtained from the data given by [Tanaka et al. \(2002\)](#). In Eq. (45) the two factors of the right hand side are respectively the saturation function of the vortensity component of the horseshoe drag, and the unsaturated horseshoe drag. The former has the expression ([Masset & Casoli 2010](#)):

$$\mathcal{F}_V = \frac{8\pi}{3} z_\nu F(z_\nu), \quad (47)$$

where $F(x)$ is defined as:

$$F(x) = \begin{cases} 1 - x^{1/2} & \text{if } x < 4/9 \\ 4/(27x) & \text{otherwise,} \end{cases} \quad (48)$$

and the latter has the expression:

$$\Gamma_V^{\text{UHD}} = \frac{3}{4} \left(\frac{3}{2} - \alpha \right) \Sigma_0 \Omega_p^2 x_s^4. \quad (49)$$

This last expression, initially established for two dimensional discs ([Ward 1991](#); [Masset 2001](#); [Casoli & Masset 2009](#)), has been generalised to three dimensional discs ([Masset & Benítez-Llambay 2016](#)). Eqs. (42), (45), (49), (46) and (47) correspond to the five cells of the first frame of Fig. 1, from left to right and bottom to top.

Next, we give the expression of the entropy component of the corotation torque, corresponding to the second frame of Fig. 1. It reads⁶:

$$\Gamma_S^{\text{CR}} = \varepsilon_\nu \varepsilon_\chi \Gamma_S^{\text{HD}} + (1 - \varepsilon_\nu \varepsilon_\chi) \Gamma_S^{\text{lin}}. \quad (50)$$

As for the vortensity torque, we keep for the blending coefficients the expressions given by [Masset & Casoli \(2010\)](#):

$$\varepsilon_\nu = [1 + (6hz_\nu)^2]^{-1} \quad (51)$$

and

$$\varepsilon_\chi = (1 + 15hz_\chi)^{-1}, \quad (52)$$

where z_χ is defined in a similar fashion as z_ν (see [Masset & Casoli 2010](#), Eq. 81):

$$z_\chi = \frac{r_p \chi}{\Omega_p x_s^3}. \quad (53)$$

The linear component of the torque, as seen in section 4.3, is:

$$\Gamma_S^{\text{lin}} = 0.8\xi\Gamma_0/\gamma, \quad (54)$$

where ξ is given by:

$$\xi = \beta - 0.4\alpha - 0.64. \quad (55)$$

The horseshoe drag Γ_S^{HD} of Eq. (50) is simply the product of the unsaturated horseshoe drag by the saturation function of the entropy corotation torque:

$$\Gamma_S^{\text{HD}} = \mathcal{F}_S \Gamma_S^{\text{UHD}}. \quad (56)$$

In two dimensions, the expression of the unsaturated horseshoe drag can be written $K\xi\Sigma_0\Omega_p^2x_s^4$, where K is a numerical constant ([Baruteau & Masset 2008](#)). We assume

this dependency to hold in three dimensions, and seek the value of K using the results of section 4.3. In the numerical exploration that we performed, we had, using Eq. (37), $x_s = 1.086r_p(q/h')^{1/2}$, from which we infer $K = 3.3$. The unsaturated torque expression is therefore:

$$\Gamma_S^{\text{UHD}} = 3.3\xi\Sigma_0\Omega_p^2x_s^4. \quad (57)$$

For the saturation function we keep the dependence given by [Masset & Casoli \(2010\)](#):

$$\mathcal{F}_S = 1.2 \times \overline{1.4z_\chi^{1/2}} \times \overline{1.8z_\nu^{1/2}}, \quad (58)$$

where $\bar{x} = \min(1, x)$. Eqs. (50), (56), (57), (54) and (58) correspond to the five cells of the second frame of Fig. 1, from left to right and bottom to top.

The third frame of Fig. 1 corresponds to the temperature component of the corotation torque, that we now evaluate:

$$\Gamma_T^{\text{CR}} = \varepsilon_\nu \Gamma_T^{\text{HD}} + (1 - \varepsilon_\nu) \Gamma_T^{\text{lin}}. \quad (59)$$

Since the vortensity distribution associated to this torque component is roughly similar to that of the entropy torque (it is concentrated near the separatrices), we assume that it behaves like the entropy torque as a function of viscosity. However, we discard the dependence on thermal diffusivity. Indeed, in the limit of a large diffusivity, the disc behaves isothermally and the temperature torque subsists (as we saw in section 4.2), on the contrary of the entropy torque. The linear component that features in Eq. (59) reads (see section 4.2):

$$\Gamma_T^{\text{lin}} = 1.0\beta\Gamma_0/\gamma, \quad (60)$$

while the horseshoe drag reads:

$$\Gamma_T^{\text{HD}} = \mathcal{F}_T \Gamma_T^{\text{UHD}}. \quad (61)$$

From the above discussion we adopt:

$$\mathcal{F}_T = 1.2 \times \overline{1.8z_\nu^{1/2}}. \quad (62)$$

For the unsaturated horseshoe drag, we assume the form $K'\beta\Sigma_0\Omega_p^2x_s^4$, i.e. similar to that of the entropy, but with a different numerical constant and a scaling on the temperature gradient. The toy model presented by [Casoli & Masset \(2009\)](#) suggests it is reasonable, at least in the low mass limit, as it displays a scaling in $x_s^2\Delta P$, where ΔP is the perturbation of pressure at the stagnation point. This quantity, in the low mass limit, scales as $\Sigma_0\Omega_p^2x_s^2$ if the stagnation point is typically at a pressure scale length away from the planet. We seek the value of K' using the results of section 4.2. In that section, we had, using Eq. (30) (rather than Eq. 37 since the disc was isothermal), $x_s = 1.13r_p(q/h)^{1/2}$. Equating the form given above with that of Eq. (13), we infer $K' = k'/1.13^4 = 0.73$ and thus:

$$\Gamma_T^{\text{UHD}} = 0.73\beta\Sigma_0\Omega_p^2x_s^4. \quad (63)$$

Eqs. (59), (61), (63), (60) and (62) correspond to the five cells of the third frame of Fig. 1, from left to right and bottom to top.

In a fourth and last stage, we evaluate the additional component, arising from the viscous creation of vortensity at the abrupt density jumps that appear at the contact discontinuities at the separatrices of the horseshoe region. For brevity and definiteness we hereafter call this term the

⁶ Note that in [Masset & Casoli \(2010\)](#), the thermal diffusivity was denoted by κ , whereas here it is denoted by χ , while κ is the opacity. As a consequence, $\varepsilon_\kappa(z_\kappa)$ has been changed into $\varepsilon_\chi(z_\chi)$.

viscous coupling term (VCT). [Masset & Casoli \(2010\)](#) give an expression of this term (the second part of the bracket of their Eq. 129). This term corresponds to an asymptotic value (at larger time) and therefore already embeds its own saturation function. It naturally scales with the entropy gradient, as it is this gradient which primarily determines the magnitude of the density jumps at the separatrices. As emphasised in section 4.3, the quantity ξ was determined from a best fit of numerical data, and named entropy gradient on the grounds of the very close resemblance of the effect studied in that section with the well-studied two-dimensional process that triggers the appearance of an additional torque component that scales with the radial entropy gradient ([Paardekooper & Papaloizou 2008](#); [Baruteau & Masset 2008](#)). We therefore suggest that the three-dimensional version of the VCT scales with ξ . Our choice of normalisation of ξ is that the coefficient of β is unity, whereas it is $-1/\gamma$ with the normalisation of [Masset & Casoli \(2010\)](#). As this torque behaves as a bulk term (it implies a smooth distribution of vortensity from corotation to the separatrices), and since it has no known linear equivalent, we follow [Masset & Casoli \(2010\)](#) and assume it to decay like the vortensity component of the horseshoe drag, proportionally to ε_b :

$$\Gamma_{\text{VCT}}^{\text{CR}} = \frac{4\pi\xi}{\gamma} \Sigma_0 \Omega_p^2 \chi_s^4 \varepsilon_b z_\nu \left[\frac{z_\nu F(z_\nu) - z_\chi F(z_\chi)}{z_\nu - z_\chi} \right] \quad (64)$$

The full corotation torque is finally given by:

$$\Gamma_C = \Gamma_V^{\text{CR}} + \Gamma_S^{\text{CR}} + \Gamma_T^{\text{CR}} + \Gamma_{\text{VCT}}^{\text{CR}}. \quad (65)$$

Eqs. (37) to (65), together with Eq. (34), provide an expression for the total tidal torque exerted on a low to intermediate mass planet in circular orbit in an optically thick disc in hydrostatic and radiative equilibrium.

5.2 Linear regime in the general case

We give hereafter the simpler expression of the torque in the linear regime. It reduces to:

$$\Gamma_{\text{tot}}^{\text{lin}} = \Gamma_L + \Gamma_V^{\text{lin}} + \Gamma_S^{\text{lin}} + \Gamma_T^{\text{lin}}, \quad (66)$$

which simplifies as:

$$\Gamma_{\text{tot}}^{\text{lin}} = \Gamma_L + (0.46 - 0.96\alpha + 1.8\beta) \frac{\Gamma_0}{\gamma}, \quad (67)$$

where Γ_L is given by Eq. (39).

5.3 Linear regime in an isothermal disc

We can further simplify this expression in the case of an isothermal disc (in which case we discard the entropy component of the corotation torque). This yields:

$$\Gamma_{\text{tot}}^{\text{lin,iso}} = -(1.36 + 0.54\alpha + 0.5\beta)\Gamma_0. \quad (68)$$

This result is in good agreement with the result obtained by [D'Angelo & Lubow \(2010, see their Eq. 9\)](#) in three-dimensional simulations of locally isothermal discs.

6 DISCUSSION

We compare here the torque value provided by our formula of section 5 to published studies of the torque value in radiative discs, either as a function of the planetary mass or of the orbital radius. Fig. 8 shows the comparison to results recently published by [Lega et al. \(2015\)](#). They show a broad agreement between the torque measured in their simulations and our torque formula. They also show that the boost of the horseshoe width, described by Eq. (37), is an essential ingredient of the torque formula above $10 - 15 M_\oplus$ (*i.e.* for intermediate mass planets), and that torque formulae based on a low-mass expression of the width of the horseshoe region hardly yield a migration reversal.

It should be kept in mind that the torque measured in numerical simulations is subjected to some inaccuracy, as can be seen from the results for $20 M_\oplus$ (in the first two plots), for which two torques values are displayed. This inaccuracy arises from a variety of numerical effects, such as resolution (in particular the number of zones over which the radial width of the horseshoe region is resolved), or the recipe for the torque calculation (in particular whether it includes all zones or whether it excludes those located near the planet), etc. Yet, some points or parts of the torque curves are outliers with respect to our formula:

- At low planetary mass (on the left plot), the torque measured is somehow below the value predicted by our formula. This behaviour was already discussed by [Lega et al. \(2015\)](#), and attributed to the “cold-finger” effect ([Lega et al. 2014](#)), which is observed on low-mass planets when there is thermal diffusion in the disc. We note that [Masset & Casoli \(2010\)](#) have obtained their Eq. (156) — here Eq. (40) — using a fit of numerical simulations with different values of the thermal diffusivity, and may have unwittingly included a two-dimensional version of the “cold-finger” effect. It is therefore unclear to which extent the discrepancy found at low planetary mass is due to this effect. We also note that for the lowest planetary mass considered here ($5 M_\oplus$), [Lega et al. \(2014\)](#) found that the cold finger effect nearly vanishes. This issue requires further work, and will be presented elsewhere.

- The plateau value for the mass range $15 - 35 M_\oplus$ on the middle plot, or the elbow of the left plot (at $38 M_\oplus$ according to our formula, and at $\sim 50 M_\oplus$ in the results of [Lega et al. \(2015\)](#)) are also discrepant features, which are unlikely to be explained by the errors and systematic effects on the torque measurement.

Beside the “cold-finger” effect, which might account for the mismatch at low mass, there is a number of simplifications in our torque formula which can explain the residual discrepancies between our torque formula and the results of numerical simulations. We neglect the feed back of the planet’s torque on the disc density profile. At intermediate masses, this feed back tends to create a dip around the orbit (precursor of the gap that would be carved at larger masses), which has an effect on the different components of the torque. In particular the effect can be different on the outer Lindblad torque and on the inner Lindblad torque, resulting in a non-trivial effect on the net Lindblad torque. Also, the slight decrease of density can alter the thermal diffusivity at the planetary orbit, by virtue of Eq. (34). On the other hand, as we saw in

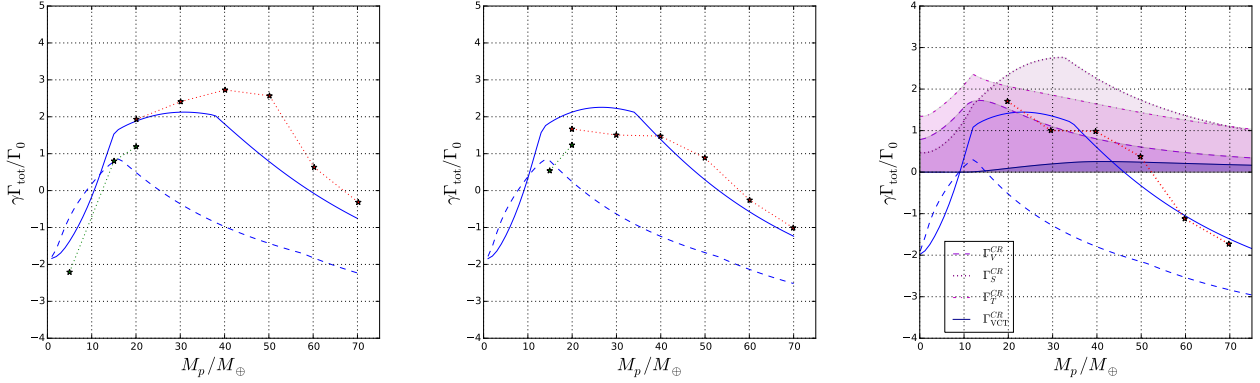


Figure 8. These figures show the comparison between our torque formula (solid line) and the results of Lega et al. (2015). Plots from left to right should be compared to Figs. 5a to 5c of that work, and show results for a standard accretion disc (SAD) model. The dashed line corresponds to the outcome of our new torque formula when one uses the relationship $x_s = 1.05\sqrt{q/h'}$ instead of Eq. (37). This shows the importance of an accurate estimate of the width of the horseshoe region for intermediate mass planets (*i.e.* here for planets above $10 M_\oplus$). In the right plot we show the different components of the corotation torque, namely the vortensity torque (dashed line), the entropy torque (dotted line), the temperature torque (dash-dotted line) and the viscous coupling term (solid line). The latter is found to be virtually negligible, whereas the first three have similar orders of magnitude. The Lindblad torque is not represented, as it is constant and off the limits of the plot : $\gamma\Gamma_L/\Gamma_0 \approx -4.6$. We thank Elena Lega for kindly providing us with the model data.

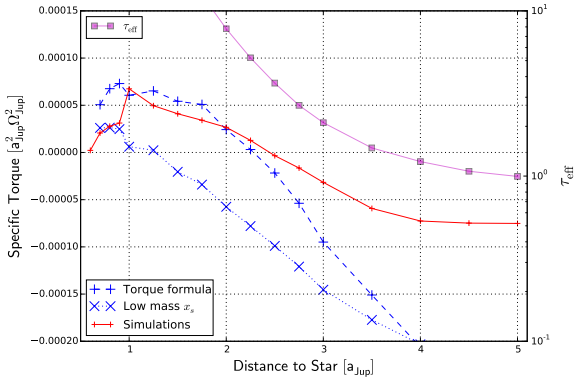


Figure 9. Comparison to the results of Bitsch & Kley (2011, hereafter BK11) for a $20 M_\oplus$ planet. The dashed line shows the result of our torque formula, the solid line with crosses (in red in the electronic version) the results obtained by BK11, and the dotted line the outcome of our torque formula when one adopts the low-mass scaling for the horseshoe width. The right vertical axis shows the effective optical depth $\tau_{\text{eff}} = \Sigma\kappa/2$ evaluated from the midplane quantities, and corresponds to the solid line with squares (in magenta in the electronic version). This figure should be compared to Figs. 2 and 3 of BK11. We thank Bertram Bitsch for kindly providing us with the model data.

section 4.5, this equation is accurate only to within $\sim 25\%$, and both the saturation functions and the blending coefficients between the linear torque and the horseshoe drag depend sensitively on the value of the thermal diffusivity. Also, we use for these functions the analytic dependence worked out in two dimensions by Masset & Casoli (2010), which can constitute another reason for the discrepancy. Lastly, we have used for all components of the corotation torque the actual adiabatic index of the gas γ , instead of an effective

adiabatic index as done for the Lindblad torque (Masset & Casoli 2010; Paardekooper et al. 2011). We comment that we have performed runs with planets of mass $1 M_\oplus$ to $20 M_\oplus$ embedded in radiative discs with different opacities (namely $1.8 \text{ cm}^2 \text{ g}^{-1}$ and $5 \text{ cm}^2 \text{ g}^{-1}$). We have found that the width of the horseshoe region at low mass corresponds indeed to $x_s = 1.05\sqrt{q/h}/\gamma^{1/4}$ rather than $x_s = 1.05\sqrt{q/h}/\gamma_{\text{eff}}^{1/4}$. At larger masses, it displays a growth above this value, as expected for the transition from the low-mass to the high-mass branch of the horseshoe width. Nonetheless, owing to thermal diffusion, the actual law might be more complex than the one of Eq. (37) and this can have an impact on the torque value, which is a very sensitive function of x_s .

We finally compare the torque predicted by our formula to that measured by Bitsch & Kley (2011) in Fig. 9. For radii below $2.5 a_{\text{Jup}}$, there is a satisfactory agreement between the formula and the numerical simulations. Beyond that radius, however, the predicted torque plummets to low values, whereas the torque measured in the simulations plateaus at an intermediate, negative value. We note that this happens when the disc's optical depth drops below value of a few (at $r = a_{\text{Jup}}$ it is $\tau_{\text{eff}} \sim 4$). Note that the actual optical depth of the disc is somehow lower than the one displayed, as the opacity law adopted by the authors was: $\kappa/(1 \text{ cm}^2 \text{ g}^{-1}) = 2.0 \cdot 10^{-4}[T/(1 \text{ K})]^2$ (Bitsch, private communication). The heat source of the disc being viscous friction, it is hotter at the midplane, and therefore its opacity is largest at the midplane. This example illustrates the fact that Eq. (34), and therefore our torque formula, are valid when the disc is optically thick. Fig. 9 also shows that torque formulae based on the low-mass scaling of the horseshoe width hardly predict any migration reversal.

We comment that the dependence of the corotation torque on viscosity and thermal diffusivity is entirely contained in the saturation functions and blending coefficients. Since those are not reconsidered in the present work, our torque has same dependence on viscosity and thermal diffu-

sivity as the dependence found by [Masset & Casoli \(2010\)](#). Namely, Figs. 13, 17 and 18 of that work show the dependence of the vortensity torque in the viscosity, and the dependence of the entropy torque on the viscosity and thermal diffusivity. The temperature term of the corotation torque was not considered in that work, but it exhibits same dependence on viscosity as the entropy torque.

7 CONCLUSION

We provide an updated formula for the torque experienced by a low mass ($q < 0.2h^3$) or intermediate mass planet ($0.2h^3 \lesssim q \lesssim 2h^3$) in circular and non-inclined orbit in an optically thick disc. Our torque formula agrees reasonably well with the torque measured in numerical simulations, as shown by comparison with recently published results. One key ingredient of the formula is an accurate expression of the width of the horseshoe region as a function of the planet-to-star mass ratio and of the disc's aspect ratio. Using in our torque formula the low-mass scaling $x_s = 1.05r_p\sqrt{q}/h$ clearly yields wrong, largely underestimated results for intermediate mass planets. We have used tailored, three-dimensional explorations of the parameter space to update several numerical coefficients that appear in the torque formula. Our work does not consider the effect found at low planetary mass by [Lega et al. \(2014\)](#) in discs with thermal diffusion, and called by these authors the “cold-finger” effect. A further step toward accurate torque formulae could be an analytic expression of this torque component, as well as a relaxation of the different simplifying assumptions mentioned in section 6.

ACKNOWLEDGEMENTS

The authors thank Elena Lega and Bertram Bitsch for an extremely careful reading of a first draft of this manuscript, and for constructive feedback. Alejandra Jiménez acknowledges financial support from a UNAM DGAPA fellowship. The simulations presented in this work were run on a GPU cluster acquired with CONACyT's grant 178377. The authors acknowledge support from UNAM's grant PAPIIT IN101616.

REFERENCES

- Baruteau C., Masset F., 2008, [ApJ](#), **672**, 1054
 Baruteau C., Masset F., 2013, in Souchay J., Mathis S., Tokieda T., eds, *Lecture Notes in Physics*, Berlin Springer Verlag Vol. 861, *Lecture Notes in Physics*, Berlin Springer Verlag. p. 201 ([arXiv:1203.3294](#)), doi:10.1007/978-3-642-32961-6_6
 Benítez-Llambay P., Masset F. S., 2016, [ApJS](#), **223**, 11
 Bitsch B., Kley W., 2010, [A&A](#), **523**, A30
 Bitsch B., Kley W., 2011, [A&A](#), **536**, A77
 Bitsch B., Crida A., Morbidelli A., Kley W., Dobbs-Dixon I., 2013, [A&A](#), **549**, A124
 Bitsch B., Morbidelli A., Lega E., Crida A., 2014, [A&A](#), **564**, A135
 Casoli J., Masset F. S., 2009, [ApJ](#), **703**, 845
 Cossou C., Raymond S. N., Hersant F., Pierens A., 2014, [A&A](#), **569**, A56
 Crida A., Morbidelli A., Masset F., 2006, [Icarus](#), **181**, 587
 D'Angelo G., Lubow S. H., 2010, [ApJ](#), **724**, 730
 Dong R., Rafikov R. R., Stone J. M., 2011, [ApJ](#), **741**, 57
 Duffell P. C., 2015, [ApJ](#), **806**, 182
 Fromang S., Lyra W., Masset F., 2011, [A&A](#), **534**, A107
 Fung J., Shi J.-M., Chiang E., 2014, [ApJ](#), **782**, 88
 Fung J., Artymowicz P., Wu Y., 2015, [ApJ](#), **811**, 101
 Fung J., Masset F., Lega E., Velasco D., 2017, [AJ](#), **153**, 124
 Kanagawa K. D., Muto T., Tanaka H., Tanigawa T., Takeuchi T., Tsukagoshi T., Momose M., 2015, [ApJ](#), **806**, L15
 Klahr H., 2004, [ApJ](#), **606**, 1070
 Kley W., 1989, [A&A](#), **208**, 98
 Kley W., Bitsch B., Klahr H., 2009, [A&A](#), **506**, 971
 Korycansky D. G., Pollack J. B., 1993, [Icarus](#), **102**, 150
 Lega E., Crida A., Bitsch B., Morbidelli A., 2014, [MNRAS](#), **440**, 683
 Lega E., Morbidelli A., Bitsch B., Crida A., Szulágyi J., 2015, [MNRAS](#), **452**, 1717
 Levermore C. D., Pomraning G. C., 1981, [ApJ](#), **248**, 321
 Masset F., 2000, [A&AS](#), **141**, 165
 Masset F. S., 2001, [ApJ](#), **558**, 453
 Masset F. S., 2002, [A&A](#), **387**, 605
 Masset F. S., Benítez-Llambay P., 2016, [ApJ](#), **817**, 19
 Masset F. S., Casoli J., 2009, [ApJ](#), **703**, 857
 Masset F. S., Casoli J., 2010, [ApJ](#), **723**, 1393
 Masset F. S., Ogilvie G. I., 2004, [ApJ](#), **615**, 1000
 Masset F. S., D'Angelo G., Kley W., 2006, [ApJ](#), **652**, 730
 Paardekooper S.-J., Papaloizou J. C. B., 2008, [A&A](#), **485**, 877
 Paardekooper S.-J., Papaloizou J. C. B., 2009a, [MNRAS](#), **394**, 2283
 Paardekooper S.-J., Papaloizou J. C. B., 2009b, [MNRAS](#), **394**, 2297
 Paardekooper S., Baruteau C., Crida A., Kley W., 2010, [MNRAS](#), **401**, 1950
 Paardekooper S., Baruteau C., Kley W., 2011, [MNRAS](#), **410**, 293
 Shakura N. I., Sunyaev R. A., 1973, [A&A](#), **24**, 337
 Tanaka H., Takeuchi T., Ward W. R., 2002, [ApJ](#), **565**, 1257
 Ward W. R., 1986, [Icarus](#), **67**, 164
 Ward W. R., 1991, in *Lunar and Planetary Institute Conference Abstracts*. p. 1463
 de Val-Borro M., et al., 2006, [MNRAS](#), pp 695+

This paper has been typeset from a $\text{\TeX}/\text{\LaTeX}$ file prepared by the author.